• Basic Research •

Mitochondrial outer membrane protein FUNDC2 contributes to ferroptosis as a potential upstream regulator in retinitis pigmentosa

Jie-Yu Chen, Ya-Fen Huang, Yu Hong

Department of Ophthalmology, The Second Affiliated Hospital of Fujian Medical University, Quanzhou 362000, Fujian Province, China

Co-first Authors: Jie-Yu Chen and Ya-Fen Huang

Correspondence to: Yu Hong. Department of Ophthalmology, The Second Affiliated Hospital of Fujian Medical University, Quanzhou 362000, Fujian Province, China. hongyuccd@163.com

Received: 2026-05-02 Accepted: 2026-05-20

Abstract

● **AIM:** To investigate the key role of the mitochondrial outer membrane protein FUN14 domain-containing 2 (FUNDC2) in retinal pigment epithelium (RPE) ferroptosis during retinitis pigmentosa (RP) progression.

● **METHODS:** Unbiased label-free proteomics was employed to identify differentially expressed proteins in the RPE of a sodium iodate (SI)-induced rat model. *In vitro* experiments were conducted using human retinal pigment epithelial (ARPE)-19 cells. The effects of SI treatment and FUNDC2 knockdown on cell viability and the expression of ferroptosis-protective molecules, including glutathione peroxidase 4 (GPX4), solute carrier family 7 member 11 (SLC7A11), ferritin heavy chain 1 (FTH1), and solute carrier family 25 member 11 (SLC25A11) were evaluated.

● **RESULTS:** Proteomic analysis revealed that FUNDC2 was significantly upregulated in the RPE of SI-induced rats. In ARPE-19 cells, SI treatment significantly increased FUNDC2 expression while decreasing the levels of ferroptosis-protective molecules. Functional experiments demonstrated that knocking down FUNDC2 effectively rescued SI-induced loss of cell viability and restored GPX4 expression.

● **CONCLUSION:** These findings provide the first evidence that FUNDC2 acts as a potential upstream regulator of RPE ferroptosis in RP, at least partially by negatively regulating GPX4. Consequently, FUNDC2 is a potential therapeutic target for the future treatment of RP.

● **KEYWORDS:** retinitis pigmentosa; ferroptosis; FUNDC2; retinal pigment epithelium; sodium iodate

DOI:10.18240/ijo.2026.09.02

Citation: Chen JY, Huang YF, Hong Y. Mitochondrial outer membrane protein FUNDC2 contributes to ferroptosis as a potential upstream regulator in retinitis pigmentosa. *Int J Ophthalmol* 2026;19(9):1667-1675

INTRODUCTION

Retinitis pigmentosa (RP) is a group of inherited retinal dystrophies (IRDs) characterized by progressive degeneration of photoreceptors and the retinal pigment epithelium (RPE)[1]. The global prevalence of the disease is about 1/3500 to 1/4500[2]. The disease is irreversible and eventually leads to severe visual impairment[3]. Although substantial progress has been made in gene therapy, there is currently no universally effective treatment for most patients[4-5].

Despite the marked genetic heterogeneity of RP, accumulating evidence suggests that dysfunction of the RPE plays a critical role in disease initiation and progression[6-7]. The RPE is essential in maintaining retinal homeostasis. Due to its high metabolic requirements and continuous exposure to photo-oxidative stress, the RPE is particularly vulnerable to oxidative damage[8]. In this context, ferroptosis, an iron-dependent and lipid peroxidation—driven form of regulated cell death, has emerged as an important mechanism implicated in retinal degeneration[9-10]. Notably, the RPE is rich in intracellular polyunsaturated fatty acids (PUFAs) and exhibits active iron metabolism, rendering it susceptible to iron-dependent lipid peroxidation under pathological conditions[11]. Consequently, ferroptosis has been identified as a major pathogenic mechanism in retinal degenerative diseases, including RP[12].

Sodium iodate (SI) is widely used to induce selective oxidative injury in RPE, leading to secondary degeneration of the neurosensory retina. This model recapitulates morphological and functional features of RP and has therefore been employed to investigate RPE-associated pathogenic mechanisms, including ferroptosis[13-14]. Previous studies have demonstrated that SI exposure can induce ferroptosis in human retinal pigment epithelial (ARPE-19) cells[15]. However, the upstream regulators of ferroptosis in RP and their mechanisms remain largely unknown.

To address this gap, we performed an unbiased label-free quantitative proteomic analysis in an SI-induced RP rat model and identified FUN14 domain-containing 2 (FUNDC2) as a significantly upregulated protein. FUNDC2 is a conserved mitochondrial outer membrane protein and is involved in multiple pathophysiological processes, including regulating apoptosis, mitophagy, and tumorigenesis[16-19]. Given that mitochondrial dysfunction is closely associated with ferroptosis[20], we hypothesized that FUNDC2 may serve as a potential molecule linking mitochondrial stress to ferroptosis. Consistently, a recent study demonstrated that FUNDC2 promotes ferroptosis in cardiomyocytes and contributes to doxorubicin-induced cardiomyopathy[21]. However, the involvement of FUNDC2 in RP and its potential role in driving RPE ferroptosis remain unexplored.

In this study, we aimed to investigate the role of FUNDC2 in RPE ferroptosis using *in vitro* models of RP and to determine whether FUNDC2 functions as a potential upstream regulator of ferroptosis. By integrating proteomic profiling with functional validation, this work seeks to identify novel targets and provide a theoretical basis for a gene-independent treatment strategy for RP.

MATERIALS AND METHODS

Ethical Approval All animal experiments were conducted in accordance with the National Standard of the People's Republic of China, "Guidelines for the Ethical Review of Laboratory Animal Welfare" (GB/T 35892-2018) and were approved by the Ethics Committee of the Second Affiliated Hospital of Fujian Medical University [Approval No. (2025) Fu Medical Second Ethics Review 207]. Additionally, all procedures are in line with the Statement on the Use of Animals in Ophthalmic and Vision Research of the Association for Research in Vision and Ophthalmology.

Animals and Establishment of RP Models Specific-pathogen-free (SPF) male Sprague-Dawley (SD) rats, aged 5–6wk, were provided by the Experimental Animal Center of Hangzhou Medical College. Animals were housed under controlled conditions (temperature 23℃±1℃, humidity 50%±5%) at the Experimental Animal Center of the Second Affiliated Hospital of Fujian Medical University, with a 12-hour light/dark cycle (lights on at 8:00 *a.m.*) and free access to standard chow and water. After 7d of acclimatization, 20 male SD rats (6–8 weeks old) were randomly assigned to the SI group (n=10) and the control group (n=10). The SI group received a single intravenous injection of 2% SI (45 mg/kg; SI, CAS 7681-55-2, Macklin, Shanghai, China), while the control group received an equal volume of 0.9% sodium chloride solution (CAS 7647-14-5, Macklin, Shanghai, China) *via* tail vein injection. During injection, the needle was inserted nearly parallel to the tail at an angle less than 15°, and the solution was administered after confirming blood reflux. One week after modeling, rats were euthanized by intraperitoneal injection of pentobarbital sodium (3%, 50 mg/kg) followed by collection of retinal tissue for further analysis.

Hematoxylin and Eosin Staining After intraperitoneal injection of sodium pentobarbital for anesthesia, perform cardiac perfusion fixation. First, perfuse physiological saline at a flow rate of 50 mL/min for 5min, then perfuse 4% paraformaldehyde (CAS 30525-89-4, Thermo Fisher Scientific, Shanghai, China) at a flow rate of 40 mL/min for approximately 10min until limb rigidity occurs. After enucleation, mark the 1 o'clock position at the limbal-scleral junction with a suture to indicate orientation. The eyeballs were then immersed in a 4% paraformaldehyde solution and fixed at 4℃ for 24h. The tissues underwent dehydration with a gradient ethanol solution, cleared with xylene, embedded in paraffin, and sectioned into 4 μm thick sagittal slices. For hematoxylin and eosin (HE) staining, paraffin sections were baked at 60℃ for 40–60min, deparaffinized in xylene, and rehydrated through a graded ethanol series (100%, 90%, 80%, and 70%) for 2min each. An HE Staining Kit (Cat. No. C0105M, Beyotime, Shanghai, China) was used. Sections were stained with hematoxylin solution for 5–15min, differentiated with 1% acidic ethanol for 30s, and counterstained with 1% ammonia solution (prepared from NH_4HCO_3, CAS 1066-33-7, Sigma-Aldrich, St. Louis, MO, USA) for 3–5min. Finally, sections were counterstained with eosin solution for 2min, dehydrated, mounted with neutral resin, and imaged using an inverted light microscope (Zeiss, Oberkochen, Germany).

Protein Extraction and Enzymatic Digestion Total protein was extracted from retinal tissue using an animal tissue protein extraction kit (Cat. No. 50010D, Thermo Fisher Scientific, Shanghai, China). Protein concentration was quantified using the BCA Protein Assay Kit (Cat. No. PC0020, Beijing Solarbio Science & Technology Co., Ltd., Beijing, China), and protein integrity was assessed by SDS-PAGE. Transfer an appropriate volume of protein solution to a 1.5 mL microcentrifuge tube. Add Dithiothreitol (DTT, CAS 3483-12-3, Sigma-Aldrich, St. Louis, MO, USA) to a final concentration of 10 mmol/L and reduce at 37℃ for 1h. Iodoacetamide (IAA, CAS 144-48-9, Sigma-Aldrich, St. Louis, MO, USA) was then added to a final concentration of 50 mmol/L, and the reaction was incubated for 1h in the dark at room temperature. Subsequently, add DTT to a final concentration of 5 mmol/L and incubate for 10min. Transfer the protein sample to a 30 kDa ultrafiltration tube and perform multiple buffer exchanges and centrifugal washes using 8 mol/L urea and 50 mmol/L ammonium bicarbonate solution. Digest the protein sample with trypsin (Cat. No. 25200072, Thermo Fisher Scientific, Waltham, MA, USA) at a 1:50 (w/w) enzyme-to-protein ratio at 37℃ for 16–20h.

The resulting peptides were desalted using C18 cartridges (Thermo Fisher Scientific, Waltham, MA, USA), lyophilized, and redissolved in 40 μL of 0.1% formic acid for peptide quantification *via* OD_{280} on a NanoDrop spectrophotometer (Thermo Fisher Scientific, Waltham, MA, USA).

Mass Spectrometry Analysis Peptide samples were separated by nano-liquid chromatography (nano-LC) using an EASY-nLC 1200 system (Thermo Fisher Scientific, Waltham, MA, USA). Mass spectrometry (MS) data were acquired on a Q Exactive HF-X mass spectrometer (Thermo Fisher Scientific, Waltham, MA, USA) operating in positive mode. The full scan mass spectra (MS1) were recorded over a mass range of 300–1550 m/z at a resolution of 120 000. Fragmentation was performed using higher-energy collisional dissociation (HCD), with MS2 spectra acquired at a resolution of 15 000 (at m/z 110).

Identification of Differentially Expressed Proteins and Bioinformatics Analysis Differentially expressed proteins (DEPs) were defined as those exhibiting a fold change (FC) ≥1.5 or ≤0.667, with an associated $P<0.05$. To determine the functional significance of DEPs, we performed Gene Ontology (GO) annotation and Kyoto Encyclopedia of Genes and Genomes (KEGG) pathway enrichment analysis. GO functional annotation and enrichment analysis were carried out using the Metascape online platform (https://metascape.org/), covering three categories: cellular component, molecular function, and biological process. KEGG pathway annotation and enrichment analysis were conducted using the KEGG database (http://www.kegg.jp/kegg/pathway.html) to identify major biochemical, metabolic, and signaling pathways. Enrichment bar plots were generated using the online tool (https://www.bioinformatics.com.cn/)[22]. The statistical significance of GO terms and KEGG pathway enrichment was evaluated based on the number of enriched proteins.

Cell Culture ARPE-19 cells were provided by Yimo Biotechnology Co., Ltd. (Xiamen, China), and cultured in DMEM/F-12 (1:1) medium (Cat. No. 11320033, Thermo Fisher Scientific, Waltham, MA, USA) supplemented with 10% fetal bovine serum (Cat. No. 16140071, Thermo Fisher Scientific, Waltham, MA, USA) and 1% penicillin/streptomycin (Cat. No. 15140122, Thermo Fisher Scientific, Waltham, MA, USA) at standard conditions (37℃, 5% CO_2).

Cell Viability Assay Seed cells at a density of 1.0×10^3 cells per well in a 96-well plate. After cells have adhered, add SI at different concentrations and incubate for 12h and 24h, respectively. Subsequently, remove the SI-containing medium and add 100 μL of fresh medium to each well. Then, add 10 μL of cell counting kit-8 (CCK-8) reagent (Cat. No. MA0218, Meilunbio, Dalian, China) to each well and incubate for 1h. Measure the optical density (OD_{450}) using a multifunctional microplate reader (Thermo Fisher Scientific, Waltham, MA, USA). This assay was utilized to plot the dose-response curve, calculate the half-maximal inhibitory concentration (IC_{50}) of SI at 24h for subsequent *in vitro* modeling, and to evaluate the changes in cell viability under different treatment conditions [control, SI, negative control (NC)+SI, and SiRNA+SI groups].

SiRNA Transfection ARPE-19 cells were randomly divided into four groups: the control group (C group, cultured in standard complete medium), experimental group (SI group, treated with SI), NC group (NC+SI group, pretreated with transfection reagent without siRNA for 24h, followed by SI intervention), and transfection group (SiRNA+SI group, ARPE-19 cells were pretreated with siRNA for 24h, followed by SI intervention). One day prior to transfection, cells were seeded at a density of 3×10^5 cells/mL (2 mL per well) in 6-well plates. SiRNA transfection was performed using the LipoFiter 3.0 transfection reagent (Hanbio, Shanghai, China). Following transfection, cells were cultured for 48h for RNA extraction and 72h for protein extraction to validate gene knockdown efficiency.

The siRNA sequences are as follows: (NC) siRNA, 5’-UUCUCCGAACGUGUCACGUTT-3’ [forward (F)], 5’-ACGUGACACGUUCGGAGAATT-3’ [reverse (R)]; (hs-FUNDC2-si) siRNA, 5’-GAAGAAGAAUGUUCUAGUATT-3’(F), 5’-UACUAGAACAUUCUUCUUCTT-3’(R).

Real-Time Quantitative Polymerase Chain Reaction Total RNA was extracted from cells using the spin column method. RNA purity was assessed by an OD_{260}/OD_{280} ratio between 1.8 and 2.0. RNA was reverse transcribed into cDNA using a Reverse Transcription Kit (Cat. No. 4368814, Thermo Fisher Scientific, Waltham, MA, USA). Real-time quantitative polymerase chain reaction (RT-qPCR) was performed using PowerUp™ SYBR™ Green Master Mix (Cat. No. A25742, Applied Biosystems; Thermo Fisher Scientific) on a QuantStudio 3 Real-Time PCR System (Applied Biosystems, Thermo Fisher Scientific). Relative mRNA expression levels were calculated using the $2^{-\Delta\Delta CT}$ method. For qPCR, primer sequences were as follows: FUNDC2, 5’-GAGACAAGCTCACCGAAAT-3’(F), 5’-AATTCCGCAAGGTCCAGTGAC-3’(R); solute carrier family 25 member 11 (SLC25A11), 5’-TCAGCGGTCTTGTCACCAC-3’(F), 5’-CAGCCCGTTCTTGTATTCCG-3’(R); ferritin heavy chain 1 (FTH1), 5’-CCCCCATTTGTGTGACTTCAT-3’(F), 5’-GCCCGAGGCTTAGCTTTCATT-3’(R); solute carrier family 7 member 11 (SLC7A11), 5’-TCTCCAAAGGAGGTTACCTGC-3’(F), 5’-AGACTCCCCTCAGTAAAGTGAC-3’(R); glutathione peroxidase 4 (GPX4),

5'-GAGGCAAGACCGAAGTAAACTAC-3'(F), 5'-CCGAACTGGTTACACGGGAA-3'(R).

Western Blotting Cultured ARPE-19 cells were washed three times with prechilled phosphate buffer saline (PBS; Gibco; Thermo Fisher Scientific, Waltham, MA, USA) and collected after digestion with 0.25% trypsin. Cells were resuspended in RIPA Lysis Buffer (Cat. No. P0013B, Beyotime, Shanghai, China) containing protease and phosphatase inhibitor cocktails (Cat. No. P1048, Beyotime) and lysed by vortexing on ice for 30min. Protein concentrations were determined using the BCA Protein Assay Kit. Equal amounts of protein (30 μg per sample) were separated by 10% sodium dodecyl sulfate polyacrylamide gel electrophoresis (SDS-PAGE) and transferred onto polyvinylidene fluoride (PVDF) membranes (Millipore, Billerica, MA, USA). The membranes were blocked with QuickBlock blocking buffer (Beyotime, Shanghai, China) for 1h and then incubated overnight at 4°C with primary antibodies against FUNDC2, GPX4, and β-actin (Proteintech Group, Inc., Wuhan, China). After washing three times with tris buffered saline Tween (TBST; 5min each), the membrane was incubated with horseradish peroxidase (HRP)-conjugated secondary antibodies (1:2500; Cell Signaling Technology, Danvers, MA, USA) at room temperature for 1h. Revealed bands using an enhanced chemiluminescence (ECL) detection kit (Thermo Fisher Scientific) and visualized them with an ImageQuant LAS4000 mini-imaging system (GE Healthcare, Chicago, IL, USA). Band intensities were quantified using ImageJ software (version 1.53; NIH, Bethesda, MD, USA), and relative protein expression levels were normalized to β-actin.

Statistical Analysis Statistical analysis was performed using SPSS 22.0 (IBM Corp., Armonk, NY, USA) and GraphPad Prism 8.0 (GraphPad Software, San Diego, CA, USA). All data were presented as mean±standard deviation (SD). The Shapiro-Wilk test was used to assess data normality. For comparisons between two groups, normally distributed data were analyzed using the student's *t*-test (for equal variances) or Welch's *t*-test (for unequal variances), while non-normally distributed data were analyzed using the Mann-Whitney *U* test. For multiple comparisons, data meeting normality and homogeneity of variance were analyzed using one-way analysis of variance (ANOVA) followed by Bonferroni post hoc tests; otherwise, Kruskal-Wallis tests followed by Dunn post hoc tests were performed. Relative mRNA expression levels obtained by RT-qPCR were calculated using the $2^{-\Delta\Delta CT}$ method. *P*-value <0.05 was considered statistically significant.

RESULTS

Sodium Iodate Successfully Induced a Rat Model of Retinitis Pigmentosa HE staining revealed that retinal structure was significantly disrupted in the SI-treated group (SI group) compared to the saline-injected control group. The RPE layer in the SI group exhibited marked thinning and morphological disorganization (Figure 1). These findings confirmed that SI successfully established a rat model of RP.

Proteomic Profiling Revealed Significant Upregulation of FUNDC2 in the RP Model Label-free quantitative proteomics analysis was performed on retinal tissue from the control group and SI group. Rigorous quality control confirmed that all samples met the required standards for downstream analyses, with no evidence of protein degradation. To identify DEPs, a volcano plot was generated (Figure 2A), revealing a total of 177 DEPs (FC>1.5, *P*<0.05), including 76 upregulated and 101 downregulated proteins (Figure 2B). Hierarchical clustering analysis further confirmed significant differences in protein expression patterns between the control and SI groups (Figure 2C). Subsequently, we performed bioinformatics analysis to determine the biological significance of the identified DEPs. GO enrichment analysis revealed that these DEPs exhibited distinct dual features of defense activation and structural damage. Upregulated proteins were significantly enriched in biological processes related to translation, ribosome assembly, and negative regulation of DNA metabolic processes. Their corresponding cellular components were mainly localized in cytosolic ribosomes, nucleosomes, and protein—DNA complexes, suggesting the activation of protein synthesis and genome stability mechanisms (Figure 2D). In contrast, downregulated proteins enriched in biological processes associated with visual perception and light stimulus response were primarily localized to the inner/outer segments and ciliary structures of retinal photoreceptor cells, consistent with structural and functional degeneration of retinal photoreceptors in RP models (Figure 2E). KEGG pathway enrichment analysis further demonstrated that upregulated pathways predominantly clustered around ribosomal biosynthesis and oxidative phosphorylation, indicating metabolic reprogramming and enhanced protein synthesis, while downregulated pathways were primarily associated with phototransduction and neurodegenerative disease pathways (Figure 2F).

Collectively, these findings indicate that retinal cells initiate systemic defense responses under oxidative stress. Given that ferroptosis primarily occurs within mitochondria and that the upregulated signaling pathways include oxidative stress and mitochondrial metabolic reprogramming (oxidative phosphorylation), we focused on FUNDC2. This mitochondrial outer membrane protein exhibited significantly increased expression (*P*<0.05, FC>1.5) and is closely associated with the regulation of mitochondrial autophagy.

Concentration- and Time-Dependent Cytotoxicity of Sodium Iodate on ARPE-19 Cells To establish standardized *in vitro* model experimental conditions, we systematically evaluated the cytotoxic effects of SI on ARPE-19 cells

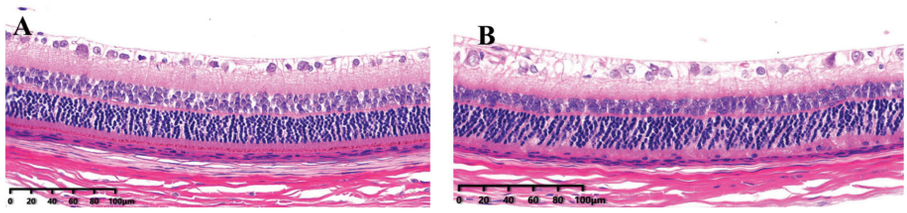

Figure 1 Histopathological assessment of SI-induced RP model in rats Rats were administered with sodium iodate (SI group) or saline (control group) *via* tail vein injection to establish the RP model, and retinal tissues were collected for HE staining 1wk after model induction. A: The retina structure of the control group was normal, with regular and orderly cellular arrangement and uniform cell density within the layers; B: The retina structure in the SI group showed severe damage, with significant thinning of the retinal pigment epithelium (RPE) layer and structural disorganization. Scale bar=100 μm. SI: Sodium iodate; RP: Retinitis pigmentosa; HE: Hematoxylin and Eosin.

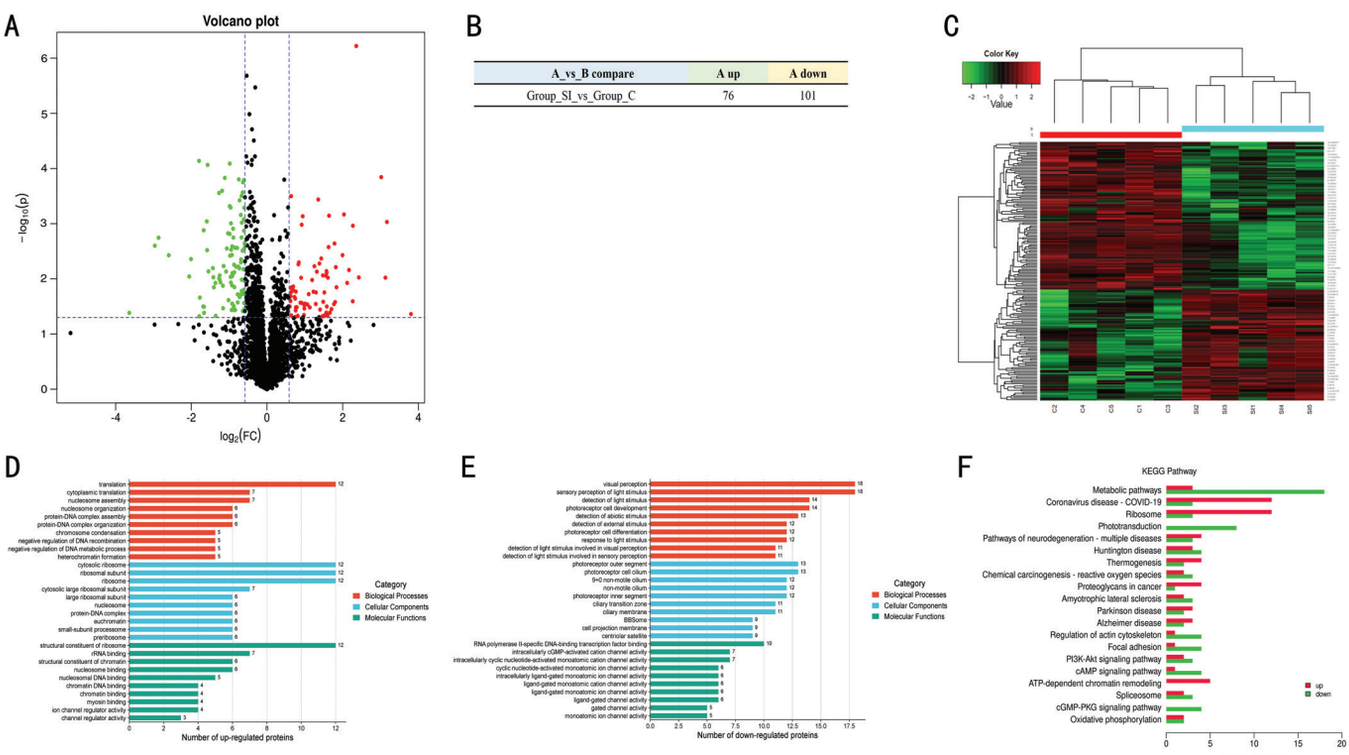

Figure 2 Proteomic screening and bioinformatic analysis of differentially expressed proteins (DEPs) A: Volcano plot of DEPs in retinal tissues. The plot displays the protein expression differences between the SI group and the C group. The x-axis represents the $\log_2$ fold change ($\log_2$FC), and the y-axis represents the negative logarithm of the *P*-value ($-\log_{10}$P). DEPs were determined using the following thresholds: FC≥1.5 and *P*<0.05 for upregulated proteins; FC≤0.667 and *P*<0.05 for downregulated proteins. Red, green, and black dots represent upregulated, downregulated, and non-significantly different proteins, respectively; B: Quantification of DEPs. A total of 177 DEPs were identified based on the selection criteria, with 76 upregulated proteins (A up, red) and 101 downregulated proteins (A down, green); C: Heatmap of DEPs. The color intensity represents the relative expression levels of proteins, with red indicating upregulation and green indicating downregulation. The heatmap shows clear clustering separation between the SI and the control groups; D and E: GO enrichment analysis of DEPs. The top 10 enriched functional terms for up- and downregulated proteins, respectively. Bars are sorted in descending order by protein count, with *P*-value as the secondary sorting criterion; F: KEGG pathway enrichment analysis of differentially expressed proteins. The bar chart shows the top enriched pathways, with red bars indicating upregulated proteins, and green bars indicating downregulated proteins. SI: Sodium iodate; FC: Fold change; GO: Gene Ontology; KEGG: Kyoto Encyclopedia of Genes and Genomes.

using the CCK-8 assay. Results demonstrated that SI exerted concentration- and time-dependent cytotoxicity on ARPE-19 cells, with increasing toxicity observed at higher concentrations and longer exposure durations (Figure 3A). Based on the dose-response curve after 24-hour treatment, we determined the half-maximal IC_{50} of SI to be 4.042 mmol/L (95%CI: 3.812–4.272 mmol/L; Figure 3B). This concentration was used as the standardized condition for all subsequent *in vitro* model experiments.

Upregulation of FUNDC2 and Downregulation of Ferroptosis Inhibitors in an *in vitro* RP Model To validate proteomics findings *in vitro,* we examined the effects of SI on

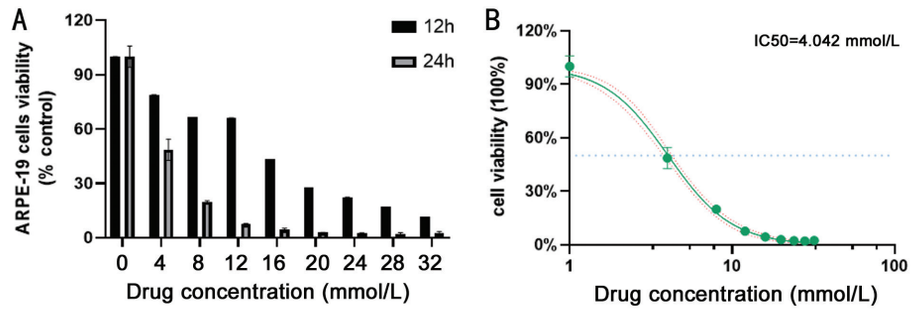

Figure 3 CCK-8 assay to assess the cytotoxicity of sodium iodate on ARPE-19 cells The CCK-8 assay was performed to evaluate the effect of sodium iodate on ARPE-19 cell viability. A: Cell viability of ARPE-19 cells at different concentrations (0 to 32 mmol/L) and time points (12 and 24h); B: Dose-response curve of ARPE-19 cell viability at 24h after treatment with different concentrations of sodium iodate, used to calculate the half-maximal inhibitory concentration (IC_{50}). CCK-8: Cell counting kit-8; ARPE: Human retinal pigment epithelial.

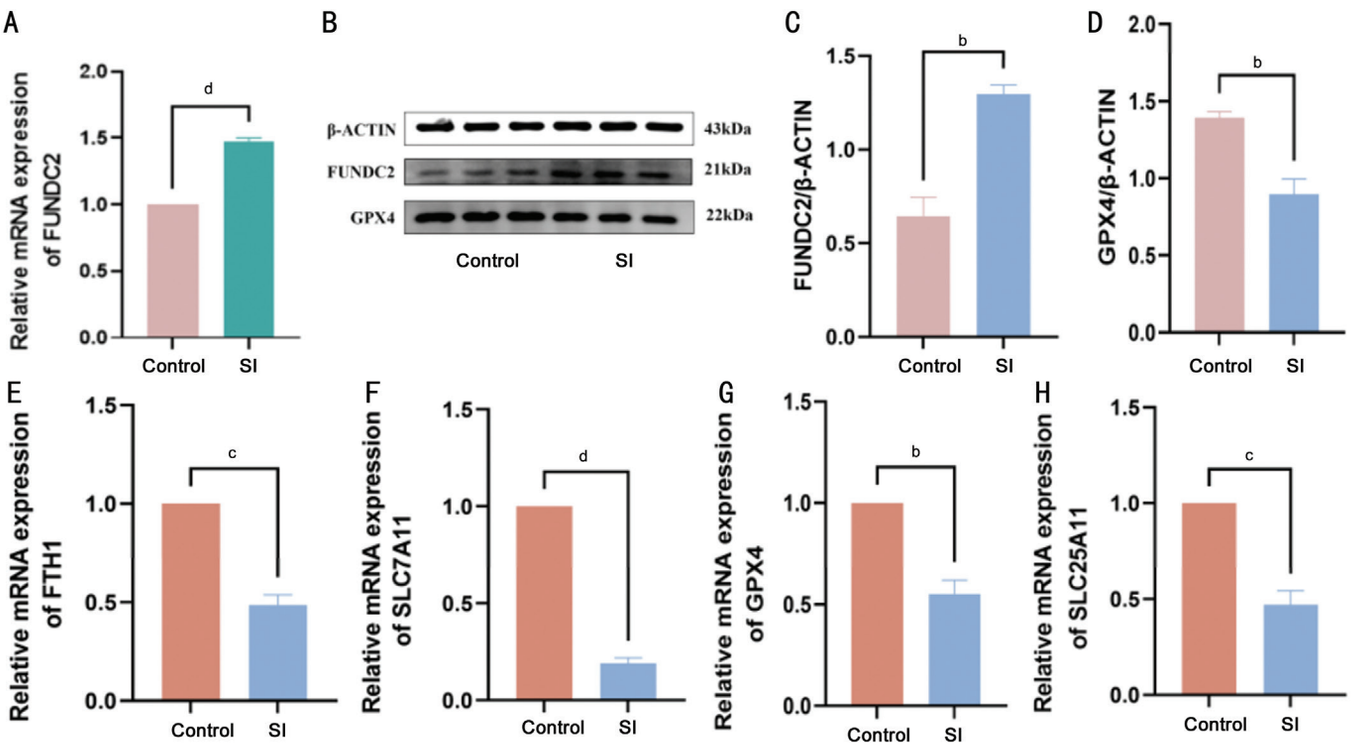

Figure 4 *In vitro* validation of SI-induced upregulation of FUNDC2 and downregulation of ferroptosis-protective molecules in ARPE-19 cells ARPE-19 cells were treated with 4.042 mmol/L sodium iodate (SI group) or saline (control group) for 24h. A–D: Validation of FUNDC2 and GPX4 expression. A: Relative mRNA expression measured by RT-qPCR; B: Western blot analysis of FUNDC2 and GPX4 protein expression; C: Quantification of FUNDC2 protein levels *via* densitometric analysis; D: Quantification of GPX4 protein levels *via* densitometric analysis; E–H: RT-qPCR analysis of mRNA levels for ferroptosis-protective genes: *FTH1* (E), *SLC7A11* (F), *GPX4* (G), and *SLC25A11* (H). β-actin served as the loading control for all protein expression analyses. Data are presented as mean±SD, with inter-group comparisons performed using Student's *t*-test. $^{b}P<0.01$, $^{c}P<0.001$, $^{d}P<0.0001$. SI: Sodium iodate; FUNDC2: FUN14 domain-containing 2; ARPE: Human retinal pigment epithelial; GPX4: Glutathione peroxidase 4; RT-qPCR: Real-time quantitative polymerase chain reaction; FTH1: Ferritin heavy chain 1; SLC7A11: Solute carrier family 7 member 11; SLC25A11: Solute carrier family 25 member 11; SD: Standard deviation.

the expression of FUNDC2 and its key ferroptosis-protective molecules in ARPE-19 cells *via* RT-qPCR and Western blot analysis. First, RT-qPCR results revealed that compared to the control group, mRNA levels of the core ferroptosis protein FUNDC2 were significantly elevated in ARPE-19 cells after 24h treatment with 4.042 mmol/L SI (SI group; Figure 4A). Western blot analysis further confirmed the significant increase in FUNDC2 protein expression in the SI group (Figures 4B and 4C). Notably, the protein levels of GPX4, a key ferroptosis inhibitor, were also significantly reduced, as confirmed by Western blot analysis (Figures 4B and 4D). Next, we evaluated the expression of ferroptosis-associated protective molecules. RT-qPCR results showed that mRNA expression levels of FTH1[23] (Figure 4E), SLC7A11[24] (Figure 4F), GPX4[25] (Figure 4G), and SLC25A11[26] (Figure 4H) were significantly downregulated following SI treatment.

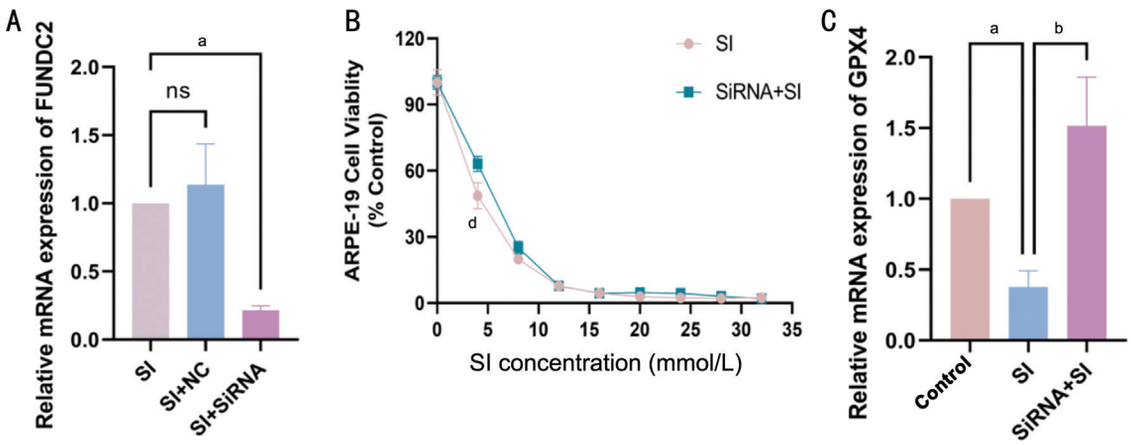

Figure 5 Effects of FUNDC2 knockdown on ARPE-19 cell viability and GPX4 expression ARPE-19 cells were divided into four groups: control (C), sodium iodate-treated (SI, 4.042 mmol/L, 24h), negative control (NC+SI), and FUNDC2 siRNA-transfected (siRNA+SI). A: Validation of FUNDC2 knockdown efficiency *via* RT-qPCR; B: CCK-8 assay for cell viability: comparison of viability between SI and siRNA+SI groups at different sodium iodate concentrations; C: RT-qPCR analysis of GPX4 mRNA expression levels across groups. Data are presented as mean±SD, with inter-group comparisons performed using one-way ANOVA. [a]*P*<0.05, [b]*P*<0.01, [d]*P*<0.0001; ns, *P*>0.05. FUNDC2: FUN14 domain-containing 2; ARPE: Human retinal pigment epithelial; GPX4: Glutathione peroxidase 4; SI: Sodium iodate; NC: Negative control; RT-qPCR: Real-time quantitative polymerase chain reaction; CCK-8: Cell counting kit-8; SD: Standard deviation; ANOVA: Analysis of Variance.

Knockdown of *FUNDC2* Restores Cell Viability and Upregulates GPX4 Expression To determine the causal role of FUNDC2 in SI-induced damage to ARPE-19 cells, the efficiency of *FUNDC2* knockdown was first validated. RT-qPCR analysis revealed significantly reduced *FUNDC2* mRNA expression in the *FUNDC2* siRNA-transfected group (SiRNA+SI group) compared to the NC group (NC+SI group; Figure 5A). CCK-8 cell viability assays revealed that SI treatment significantly reduced ARPE-19 cell viability in a dose-dependent manner, while *FUNDC2* knockdown significantly restored cell viability at the tested concentrations (Figures 5B). Finally, we investigated the effect of FUNDC2 knockdown on GPX4, a ferroptosis-inhibiting molecule. RT-qPCR results revealed that FUNDC2 silencing significantly increased GPX4 mRNA expression compared to the SI group (Figure 5C).

Taken together, our findings provide the first evidence that FUNDC2 is upregulated in RP models and may promote ferroptosis in RPE cells by negatively regulating GPX4. This discovery suggests that FUNDC2 could serve as a potential therapeutic target for RP, offering a novel direction for developing gene-independent treatment strategies.

DISCUSSION

RP is a blinding retinal disease characterized by high genetic heterogeneity, and its main clinical challenge is the lack of a universal molecular therapeutic target for most patients[1,4]. In recent years, ferroptosis, a newly identified form of programmed cell death, has become increasingly recognized as a key contributor to RP pathological progression[9,12,27]. However, its upstream regulatory mechanisms remain largely unclear. In our study, we first established a pathological association between the mitochondrial outer membrane protein FUNDC2 and RP, revealing that FUNDC2 was an upstream regulator of ferroptosis in RPE cells during RP progression. Then, using label-free quantitative proteomic analysis, we found significant upregulation of FUNDC2 expression in the SI-induced RP rat model.

Consistent with these proteomics results, subsequent *in vitro* experiments demonstrated that SI treatment significantly increased FUNDC2 expression in ARPE-19 cells at both the transcriptional and translational levels (Figures 4A–4C). More importantly, FUNDC2 overexpression consistently accompanied significant downregulation of ferroptosis protective molecules, including FTH1, SLC7A11, GPX4, and SLC25A11 (Figures 4E–4H). This observation indicates a potential correlation between FUNDC2 overexpression and ferroptosis induction in an *in vitro* RP model. These findings provide evidence and ideas for subsequent studies investigating the mechanistic link between FUNDC2 and ferroptosis.

FUNDC2 is a mitochondrial outer membrane protein whose localization and function suggest the existence of deeper molecular regulatory mechanisms. In the SI model, we found that both the mitochondrial glutathione (GSH) transporters SLC25A11 and GPX4 were significantly downregulated (Figures 4F–4G). Given that SLC25A11 is a key protein responsible for transporting GSH into the mitochondrial matrix[28] and that mitochondrial GSH is critical for maintaining mitochondrial membrane potential and reactive oxygen species (ROS) scavenging[29], it is highly noteworthy that FUNDC2 has been reported to regulate the GPX4-GSH

axis by affecting SLC25A11 protein stability[21]. Based on these literature findings, we hypothesize that FUNDC2 may inhibit the function of SLC25A11 through indirect interaction, thereby exerting its effects in retinal pigment epithelial cells. Dysfunction of SLC25A11 may lead to depletion of mitochondrial GSH, further compromising mitochondrial antioxidant capacity and indirectly or directly inhibiting GPX4 function. This exacerbates lipid peroxidation, ultimately promoting ferroptosis in RPE cells. Additionally, FUNDC2 is a homolog of the mitophagy-related protein FUNDC1[30]. Previous studies indicated that FUNDC1 regulated liver ferroptosis through a mitochondrial autophagy-dependent mechanism[31], suggesting that FUNDC2 may also regulate mitochondrial quality control, exacerbate mitochondrial damage, increase ROS production, and thereby promote ferroptosis.

We also confirmed that FUNDC2 acted as a pro-ferroptotic regulator in SI-induced RPE cell injury. Functional analysis revealed that *FUNDC2* knockdown significantly reversed SI-induced cell death and markedly enhanced cell viability (Figure 5B). Importantly, at the mechanistic level, we found that FUNDC2 expression negatively correlates with GPX4 expression. Specifically, silencing *FUNDC2* significantly upregulated *GPX4* mRNA expression (Figure 5C). GPX4 exerts a crucial ferroptosis inhibitory role by reducing lipid hydroperoxides to non-toxic lipid alcohols, thereby preventing lipid peroxidation and cell death[32-34]. As a mitochondrial outer membrane protein, FUNDC2 has previously been reported to promote ferroptosis in cardiomyocytes by negatively regulating GPX4 expression[21]. Consistent with this, our study also revealed such a correlation, demonstrating that FUNDC2 may promote ferroptosis in RPE cells by negatively regulating GPX4 expression and impairing the antioxidant capacity of the GPX4-GSH axis.

However, our study has limitations. First, our mechanistic exploration is primarily based on *in vitro* experiments. Although we have elucidated the regulatory role of FUNDC2 at the cellular level, interventions targeting FUNDC2 in *in vivo* models (*e.g.*, RP rats or genetic models) are currently lacking. Second, although our proposed mechanism linking FUNDC2 to the GPX4 axis is highly logical, direct experimental evidence, such as co-immunoprecipitation (Co-IP), co-localization analysis, or functional rescue experiments, was not performed in this work to definitively confirm the physical interaction between these proteins. Furthermore, key ferroptosis markers, including GSH levels, mitochondrial ROS, and lipid peroxidation products [such as malondialdehyde (MDA) or 4-hydroxynonenal (4-HNE)], were not directly quantified. Therefore, the precise biochemical mechanisms whereby FUNDC2 drives RPE ferroptosis remain speculative based on our current data. Future studies are warranted to fully elucidate the pro-ferroptotic role of FUNDC2 in SI-induced RP. Nevertheless, this correlative finding provides a foundation and new ideas for future research.

In summary, our study establishes the first link between the mitochondrial outer membrane protein FUNDC2 and ferroptosis in RP. By integrating proteomics and functional experiments, we demonstrate that FUNDC2 may serve as a potential upstream regulator of ferroptosis in retinal pigment epithelial cells during the progression of RP, thereby identifying a potential new therapeutic target for this condition.

ACKNOWLEDGEMENTS

We thank the Experimental Animal Center of Hangzhou Medical College for providing the SPF SD rats. We also thank the Experimental Animal Center of the Second Affiliated Hospital of Fujian Medical University for providing the animal housing and the facilities required for our experiments.

Authors' Contributions: Chen JY and Huang YF contributed equally to this work. Chen JY conceptualized the study, performed the investigation, and curated the data; Huang YF conducted formal analysis, performed visualization, interpreted the data, and drafted the manuscript; Hong Y acquired funding, supervised the study, and contributed to writing, review, and editing. All authors have read and approved the final manuscript.

Data Availability Statement: The datasets generated and analyzed during the current study are available from the corresponding author on reasonable request.

AI-Generated Content Disclosure: The authors declare that no generative artificial intelligence (AI) was used in the creation of this manuscript.

Foundations: Supported by the Natural Science Foundation of Fujian Province (No.2025J01839); Joint Funds for Scientific and Technological Innovation of Fujian Province (No.2025Y9447); Quanzhou Science and Technology Plan Project (No.2021N036S).

Conflicts of Interests: Chen JY, None; **Huang YF**, None; **Hong Y**, None.

REFERENCES

1 Hartong DT, Berson EL, Dryja TP. Retinitis pigmentosa. *Lancet* 2006;368(9549):1795-1809.

2 Hanany M, Shalom S, Ben-Yosef T, *et al*. Comparison of worldwide disease prevalence and genetic prevalence of inherited retinal diseases and variant interpretation considerations. *Cold Spring Harb Perspect Med* 2024;14(2):a041277.

3 Napoli D, Di Marco B, Salamone G, *et al*. Keeping the lights on: a new role for an old drug to support cone survival in retinitis pigmentosa. *Prog Retin Eye Res* 2025;109:101403.

4 Verbakel SK, van Huet RAC, Boon CJF, *et al*. Non-syndromic retinitis pigmentosa. *Prog Retin Eye Res* 2018;66:157-186.

5 Dias MF, Joo K, Kemp JA, *et al*. Molecular genetics and emerging therapies for retinitis pigmentosa: basic research and clinical perspectives. *Prog Retin Eye Res* 2018;63:107-131.

6 Redmond TM, Yu S, Lee E, *et al*. Rpe65 is necessary for production of 11-*cis*-vitamin A in the retinal visual cycle. *Nat Genet* 1998;20(4):344-351.

7 Gal A, Li Y, Thompson DA, *et al*. Mutations in MERTK, the human orthologue of the RCS rat retinal dystrophy gene, cause retinitis pigmentosa. *Nat Genet* 2000;26(3):270-271.

8 Wang SS, Li WH, Chen M, *et al*. The retinal pigment epithelium: Functions and roles in ocular diseases. *Fundam Res* 2024;4(6):1710-1718.

9 Dixon SJ, Lemberg KM, Lamprecht MR, *et al*. Ferroptosis: an iron-dependent form of nonapoptotic cell death. *Cell* 2012;149(5):1060-1072.

10 Dixon SJ, Olzmann JA. The cell biology of ferroptosis. *Nat Rev Mol Cell Biol* 2024;25(6):424-442.

11 Lewandowski D, Sander CL, Tworak A, *et al*. Dynamic lipid turnover in photoreceptors and retinal pigment epithelium throughout life. *Prog Retin Eye Res* 2022;89:101037.

12 Naquin ER, Garg R, Chen WJ, *et al*. Iron: more than meets the eye. *Nutrients* 2025;17(18):2964.

13 Wang JM, Iacovelli J, Spencer C, *et al*. Direct effect of sodium iodate on neurosensory retina. *Invest Ophthalmol Vis Sci* 2014;55(3):1941.

14 Enzmann V, Row BW, Yamauchi Y, *et al*. Behavioral and anatomical abnormalities in a sodium iodate-induced model of retinal pigment epithelium degeneration. *Exp Eye Res* 2006;82(3):441-448.

15 Liu BH, Wang WY, Shah A, *et al*. Sodium iodate induces ferroptosis in human retinal pigment epithelium ARPE-19 cells. *Cell Death Dis* 2021;12(3):230.

16 Li SF, Han SX, Zhang Q, *et al*. FUNDC2 promotes liver tumorigenesis by inhibiting MFN1-mediated mitochondrial fusion. *Nat Commun* 2022;13(1):3486.

17 Ma Q, Zhu CZ, Zhang WL, *et al*. Mitochondrial PIP3-binding protein FUNDC2 supports platelet survival *via* AKT signaling pathway. *Cell Death Differ* 2019;26(2):321-331.

18 Zuidema D, Jones A, Song WH, *et al*. Identification of candidate mitochondrial inheritance determinants using the mammalian cell-free system. *Elife* 2023;12:RP85596.

19 Yin LY, Cao RX, Liu ZQ, *et al*. FUNDC2, a mitochondrial outer membrane protein, mediates triple-negative breast cancer progression *via* the AKT/GSK3β/GLI1 pathway. *Acta Biochim Biophys Sin (Shanghai)* 2023;55(11):1770-1783.

20 Gan BY. Mitochondrial regulation of ferroptosis. *J Cell Biol* 2021;220(9):e202105043.

21 Ta N, Qu CR, Wu H, *et al*. Mitochondrial outer membrane protein FUNDC2 promotes ferroptosis and contributes to doxorubicin-induced cardiomyopathy. *Proc Natl Acad Sci U S A* 2022;119(36):e2117396119.

22 Tang DD, Chen MJ, Huang XH, *et al*. SRplot: a free online platform for data visualization and graphing. *PLoS One* 2023;18(11):e0294236.

23 Cui J, Chen Y, Yang Q, *et al*. Protosappanin a protects DOX-induced myocardial injury and cardiac dysfunction by targeting ACSL4/FTH1 axis-dependent ferroptosis. *Adv Sci (Weinh)* 2024;11(34):e2310227.

24 Koppula P, Zhuang L, Gan BY. Cystine transporter SLC7A11/xCT in cancer: ferroptosis, nutrient dependency, and cancer therapy. *Protein Cell* 2021;12(8):599-620.

25 Li HO, Sun YS, Yao YM, *et al*. USP8-governed GPX4 homeostasis orchestrates ferroptosis and cancer immunotherapy. *Proc Natl Acad Sci U S A* 2024;121(16):e2315541121.

26 Qi YQ, Chen L, Ding SS, *et al*. Neutrophil extracellular trap-induced ferroptosis promotes abdominal aortic aneurysm formation *via* SLC25A11-mediated depletion of mitochondrial glutathione. *Free Radic Biol Med* 2024;221:215-224.

27 Yang M, Tsui MG, Tsang JKW, *et al*. Involvement of FSP1-CoQ10-NADH and GSH-GPx-4 pathways in retinal pigment epithelium ferroptosis. *Cell Death Dis* 2022;13(5):468.

28 Chen ZF, Lash LH. Evidence for mitochondrial uptake of glutathione by dicarboxylate and 2-oxoglutarate carriers. *J Pharmacol Exp Ther* 1998;285(2):608-618.

29 Chen TH, Wang HC, Chang CJ, *et al*. Mitochondrial glutathione in cellular redox homeostasis and disease manifestation. *Int J Mol Sci* 2024;25(2):1314.

30 Qiu XR, Wang SY, Li CL, *et al*. Expression and immunological role of FUNDC2 in pan-cancer. *PLoS One* 2025;20(4):e0319343.

31 Bi YG, Liu SL, Qin X, *et al*. FUNDC1 interacts with GPx4 to govern hepatic ferroptosis and fibrotic injury through a mitophagy-dependent manner. *J Adv Res* 2024;55:45-60.

32 Zhang W, Liu Y, Liao Y, *et al*. GPX4, ferroptosis, and diseases. *Biomed Pharmacother* 2024;174:116512.

33 Seibt TM, Proneth B, Conrad M. Role of GPX4 in ferroptosis and its pharmacological implication. *Free Radic Biol Med* 2019;133:144-152.

34 Ma TY, Du JT, Zhang YF, *et al*. GPX4-independent ferroptosis—a new strategy in disease's therapy. *Cell Death Discov* 2022;8:434.